

Dynamical Phase Transition in a Fully Frustrated Square Josephson Array

K. D. Fisher, D. Stroud, and L. Janin

Department of Physics, The Ohio State University, Columbus, Ohio 43210

(April 14, 2017)

We study dynamical phase transitions at temperature $T = 0$ in a fully frustrated square Josephson junction array subject to a driving current density which has nonzero components i_x, i_y parallel to *both* axes of the lattice. Our numerical results show clear evidence for *three* dynamical phases: a pinned vortex lattice characterized by zero time-averaged voltages $\langle v_x \rangle_t$ and $\langle v_y \rangle_t$, a “plastic” phase in which both $\langle v_x \rangle_t$ and $\langle v_y \rangle_t$ are nonzero, and a moving lattice phase in which only one of the time-average voltage components is nonzero. The last of these has a finite transverse critical current: if a current is applied in the x direction, a nonzero transverse current density i_y is required before $\langle v_y \rangle_t$ becomes nonzero. The voltage traces in the moving lattice phase are periodic in time. By contrast, the voltages in the plastic phase have continuous power spectra which are weakly dependent on frequency. This phase diagram is found numerically to be qualitatively unchanged by the presence of weak disorder. We also describe two simple analytical models which recover some, but not all, the characteristics of the three dynamical phases, and of the phase diagram calculated numerically.

74.60.Ge,74.76.-w,74.50.+r,74.60.Jg

I. INTRODUCTION

There has recently been considerable interest in dynamical phases in superconductors. Such interest has been stimulated by much evidence (both theoretical and experimental) that vortex lattices, as well as other ordered systems, can exhibit various types of transitions from one type of dynamical phase to another, as a function of controllable external parameters, such as driving force and temperature. In the case of Type-II superconductors in a magnetic field, the driving force which acts on the vortex lattice is the applied current.

In disordered superconducting films and crystals, there now appear to exist at least three distinct phases, as a function of driving current and temperature [1–6]. At low driving current, the vortex lattice is pinned, and typically exhibits a glass-like order because of the random pinning centers which prevent the lattice from moving. At intermediate driving currents, the glass phase is depinned, and starts to move; this motion is thought to occur inhomogeneously in disordered superconductors (that is, some of the vortices move through random channels, while other vortices remain pinned). In this phase, the vortex system is usually said to exhibit *plastic flow*. Finally, at high driving currents, an event resembling a phase transition occurs, and the vortex system reverts back to an ordered state which closely resembles a moving crystalline phase. Most workers now believe that this third phase, especially in two dimensions, lacks long-range crystalline order but instead exhibits hexatic or smectic order, modified by the static disorder of the system [7,8]. This high-current phase is also thought to exhibit a *finite transverse critical current*, i. e., once moving parallel to the driving force, the lattice requires a finite driving force perpendicular to the average direction of motion before acquiring a nonzero transverse velocity. The details of all these phases, as well as the transitions between them, remain the subjects of much experimental and theoretical investigation.

Recently, there has been evidence that some similar behavior is to be found in *ordered* systems, both in two and three dimensions (2D and 3D). Extensive numerical studies have been carried out by Nori and collaborators, who have found a very complex structure of ordered and disordered (sometimes called “plastic”) phases as a function of the relative density of vortices and pinning sites, and of the direction of applied current relative to the axes of the periodic pinning lattice [9,10]. Some of the observed structure can be described in terms of nomenclature frequently used for incommensurate dynamical systems, such as devil’s staircases, Ar’nold tongues, etc. These workers use a standard model whereby the vortices interact with each other via a pairwise potential involving a modified Bessel function, and with the pins by a suitable short-range pinning potential. A similar model had been used previously to study vortex lattices driven through a *disordered* array of pins [11]. This earlier calculation revealed a somewhat simpler structure with three phases apparent: a pinned vortex lattice, a moving plastic phase, and a moving vortex lattice with a finite transverse critical current.

In this paper, we investigate the possibility of dynamical phase transitions in a widely investigated model system: the overdamped square Josephson junction array in a transverse magnetic field. This study is complementary to the work mentioned above, in that the phase angles of the complex superconducting order parameter are explicitly included as degrees of freedom. Although such ordered Josephson junction arrays have, of course, been extensively studied [12], little attention has been paid to the possibility of plastic phases in these materials. Strongly disordered

arrays have recently been shown numerically to have both plastic and moving-lattice phases separated by a phase boundary which appears to exhibit critical phenomena associated with a diverging correlation length [13]. Weakly disordered driven periodic systems are also predicted to have a nearly periodic temporal order at large values of the driving parameter [14].

In order to search for possible dynamical phases, we study this system in a regime in which a current is applied with nonzero components parallel to *both* the x and y axes of the array. We consider only the so-called fully-frustrated case with exactly $1/2$ flux quantum per plaquette of the square array. Even in this ordered array, we find three phases. These are (*A*) the pinned vortex lattice, (*B*) a moving lattice, and (*C*) a plastic phase occurring at currents between *A* and *B*. Phases *A* and *B* have been much discussed previously, but phase *C* seems not to have been observed in an ordered lattice. The plastic phase *C* is characterized by aperiodic voltage noise and an absence of long range vortex order. By contrast, the moving lattice *B* is characterized by voltage signals which are periodic in time, and, most strikingly, by a finite transverse critical current.

In an attempt to understand our numerical results, we also present some simple analytical models. One model is based on the assumption that the dynamics can be characterized in terms of periodically repeating 2×2 unit cells driven by a current applied at an angle to the cell axes. A second model considers the motion of a single vortex through the periodic potential formed by the lattice of Josephson-coupled grains. Both models give rise to distinct regimes in which none, one, or both of the voltage components parallel to the cell axes are nonzero. Thus, in particular, a nonzero transverse critical current is present in both analytical models.

The remainder of this paper is organized as follows. In Section II, we briefly review our calculational model. Our numerical results are presented in Section III. Section IV is an interpretive discussion which includes the two analytical models mentioned above. Our conclusions are described in Section V.

II. MODEL

In all our simulations, we take as the starting point the well-known dynamical equations for an overdamped Josephson junction array in a transverse magnetic field. We assume that each Josephson junction is resistively shunted, and we neglect the loop inductance; that is, we assume that the magnetic field generated by the currents is negligible compared to the applied magnetic field. The equations then take the form

$$I_{ab} = I_{c,ab} \sin(\phi_a - \phi_b - A_{ab}) + \frac{\hbar}{2eR_{ab}} \frac{d}{dt}(\phi_a - \phi_b - A_{ab}), \quad (1)$$

$$\sum_b I_{ab} = I_a^{ext}. \quad (2)$$

Here $I_{c,ab}$ is the critical current of the junction connecting grains a and b , R_{ab} is the shunt resistance of that junction, and I_a^{ext} is the external current fed into the a th grain. We assume a constant, uniform external field $\mathbf{B} = B\hat{z}$ perpendicular to the array, and make the gauge choice $\mathbf{A} = Bx\hat{y}$. The phase factor

$$A_{ab} = \frac{2\pi}{\Phi_0} \int \mathbf{A} \cdot d\mathbf{s} \quad (3)$$

is then easily expressed in terms of $f = Ba^2/\Phi_0$, the frustration or flux per plaquette of dimension $a \times a$, where $\Phi_0 = hc/2e$ is the flux quantum.

The equations of motion can be put in dimensionless form with the definitions $i_{ab} \equiv I_{ab}/I_c$, $i_{c,ab} \equiv I_{c,ab}/I_c$, and $g_{ab} \equiv R/R_{ab}$, and the natural time unit $\tau \equiv \frac{\hbar}{2eRI_c}$, where I_c and R are a typical critical current and a typical shunt resistance. The result of this substitution is

$$i_{ab} = i_{c,ab} \sin(\phi_a - \phi_b - A_{ab}) + \tau g_{ab} \frac{d}{dt}(\phi_a - \phi_b), \quad (4)$$

$$\sum_b i_{ab} = i_a^{ext}. \quad (5)$$

Combining these equations yields a set of coupled differential equations which is easily reduced to matrix form and solved numerically [15]. In our work, we employed a fourth-order embedded Runge-Kutta integration with variable time step [16].

In most of our calculations, we have considered a lattice without disorder: all shunt resistances $R_{ab} = R$ (or $g_{ab} = 1$), and all critical currents $i_{c,ab} = 1$ on a square array. Our array is driven by nonzero current densities in both the x and y directions: a current i_x is fed into each grain along the left-hand edge of the array, and extracted from each grain on the right-hand edge, and a current i_y is similarly injected into each grain on the bottom edge and extracted from each grain on the top edge of the array (see Fig. 1).

Starting from randomized initial phases, we integrate these equations of motion over an “equilibration” interval of 100τ - 5000τ , followed by an averaging period of 100τ - 2000τ . Typically, the external currents i are ramped up or down (in steps of 0.001 to 0.1) without rerandomizing the phases. We calculate the spatially averaged but time-dependent voltage difference $v(t') = V(t')/NRI_c$ (where $t' = t/\tau$ is the dimensionless time) between the input and output edges of the array in both the x and y directions, as well as its time-average $\langle v \rangle_t$, in both directions. In some regions of the phase diagram, these voltages appear to be periodic in time, as revealed by an analysis of the power spectrum of the voltage. In other regions, as described below, this power spectrum reveals that the voltage is aperiodic. In some of our simulations, we also tracked the number and motion of vortices in the array. The vortex number in a given plaquette α is an integer $n_{v,\alpha}$ defined by the relation

$$n_{v,\alpha} \equiv \frac{1}{2\pi} \sum_{ab} (\phi_a - \phi_b - A_{ab}) = 0, \pm 1, \quad (6)$$

where the sum is taken clockwise around the α^{th} plaquette, and each phase difference is restricted to the range $[-\pi, \pi]$. Our calculations are carried out exclusively for a frustration $f = 1/2$, i. e., an applied magnetic field equal to one flux quantum for every two plaquettes. In a square Josephson array, the ground state of this field is the well-known checkerboard vortex pattern, shown schematically in Fig. 1. Our simulations reproduce this pattern.

III. RESULTS

The central results of our calculations are summed up concisely in Fig. 2, which shows the “dynamical phase diagram” for two square Josephson junction arrays with no disorder at $f = 1/2$, driven by two orthogonal currents i_x and i_y . We find *three different phases*: a pinned vortex lattice (time-averaged voltages $v_x = v_y = 0$), a plastic flow regime ($v_x = 0, v_y > 0$ or $v_y = 0, v_x > 0$), and a moving vortex lattice ($v_x > 0, v_y > 0$). The calculated boundaries are shown in Fig. 2.

The results of Fig. 2 were obtained by two different methods. In the first procedure, the longitudinal current i_x was first ramped up from zero to a finite value, with i_y held at zero. Next, the transverse current i_y was ramped up at fixed i_x . To determine the phase boundaries, we simply searched for the currents at which the time averages $\langle v_x \rangle_t$ or $\langle v_y \rangle_t$ (or both) became nonzero. In the second method, we ramped up i_x and i_y simultaneously, holding the ratio i_y/i_x fixed. Both methods generally gave similar phase boundaries. Likewise, we found little indication of substantial hysteresis, except in determining the boundary between phases *A* and *C*. In this case, if the integration time is too long, the system tended to jump abruptly back and forth between the two phases.

We refer to the phase in which both voltages are nonzero as a “plastic” phase, by analogy with a similar phase exhibited by vortices in systems with quenched disorder. In this phase, $v(t')$ is apparently non-periodic in time; the corresponding voltage power spectrum is only weakly frequency-dependent (see below). Although we use the nomenclature of plastic, we have not checked that the vortex motion in this phase is inhomogeneous (i. e. that only some vortices are in motion while others remain pinned in this phase). Such inhomogeneous motion is thought to occur in disordered systems [11]. By contrast, in the driven lattice phase, where only $\langle v_x \rangle_t$ or $\langle v_y \rangle_t$ is nonzero, the power spectra of the voltage traces are sharply peaked at a fundamental frequency and its harmonics. Further, while one voltage is always nonzero, the other voltage is periodic, only *averaging* to zero over a cycle. We interpret this behavior as representing a vortex lattice being driven transverse to the larger of the two current components.

Various minor numerical difficulties sometimes interfered with the calculations, but they could usually be overcome. For example, spurious voltage jumps were occasionally observed during these calculations; these jumps (unlike genuine jumps) could generally be eliminated by changing the initial conditions, the integration time, or the direction of current ramping. Only those voltage jumps which appeared at the same position on the phase diagram in different runs were deemed to be genuine. From the occurrence of these jumps, however, we conclude that at certain points on the phase diagram there are several metastable dynamical states which have similar energies. The occurrence of such states may suggest a first-order transition across the phase boundary, at least in the ordered system.

In Fig. 3, we show time-dependent voltage traces at several points in the plastic and moving-lattice phases. The traces are plainly very different in the two phases. In the moving-lattice phase, the voltage traces are evidently periodic in time. By contrast, in the plastic phase, the voltages, both in x and y directions, are obviously aperiodic. Another striking feature is apparent in the moving lattice phase. In this phase, as noted above, there is a non-zero

time averaged voltage only along one of the two directions, even though current is applied along both the x and y directions. Despite this feature, there is a finite *time-dependent* voltage in the y direction, which averages to zero, and which is periodic like $v_x(t')$.

To learn more about the harmonic content of these voltage traces, we have also calculated the *voltage power spectrum* $P(\omega\tau)$, using the non-normalized Lomb method for variable-time-step data [17]:

$$P(\omega\tau) = 1/2 \left\{ \frac{\left[\sum_j (v_j - \bar{v}) \cos \omega (t_j - t_o) \right]^2}{\sum_j \cos^2 \omega (t_j - t_o)} + \frac{\left[\sum_j (v_j - \bar{v}) \sin \omega (t_j - t_o) \right]^2}{\sum_j \sin^2 \omega (t_j - t_o)} \right\}, \quad (7)$$

where t_o is defined by

$$\tan (2\omega t_o) = \frac{\sum_j \sin 2\omega t_j}{\sum_j \cos 2\omega t_j}. \quad (8)$$

Here, ω is the angular frequency, the t_j 's are the times at which the voltage is recorded, $v_j = v(t_j)$, and \bar{v} is the arithmetic average of the v_j 's. We have carried out this calculation for several points in the plastic and moving-lattice phases as indicated by triangles in Fig. 2(b). The results are shown in Fig. 4 for both v_x and v_y . Clearly, the noise confirms that the voltage in the moving-lattice phase is periodic in time, while that in the plastic phase has a continuous spectrum which is relatively weakly dependent on frequency.

The moving-lattice phase is characterized by a fundamental angular frequency ω_0 . It is readily shown that ω_0 is related to the time-averaged voltage drop across the array, $\langle V \rangle_t$, by

$$\omega_0 = 2e\langle V \rangle_t / \hbar \quad (9)$$

This relation is consistent with the widely-accepted egg-carton picture of the vortex lattice in the moving phase [18]. In this picture, the vortex lattice is viewed as a collection of eggs moving in a potential similar to an egg-carton, consisting of a periodic distribution of wells on a square lattice (each well lying at the center of a plaquette formed by four grains). During one period, the vortex lattice moves by one row through the egg-carton potential. Since there is a phase slip of 2π between two opposite edges of the array each time a vortex crosses the line joining those two edges, one can readily deduce the above relationship.

Fig. 2(a) shows that a finger of the driven lattice phase is interposed between the pinned and plastic flow phases in a 10×10 array. This finger appears to be a finite-size artifact, because it is absent in the phase diagram for a 20×20 array shown in Fig. 2(b). We believe that the phase diagram of Fig. 2(b) is likely to persist in an $N \times N$ lattice even at very large N . Thus, the ordered array at $f = 1/2$ has three phases: pinned lattice, moving plastic phase, and moving lattice.

Since a realistic Josephson lattice is certain to have some disorder, we have also carried out a limited number of calculations for an array at $f = 1/2$ with weak disorder in the critical currents. Specifically, we assume that the critical currents are independent random variables uniformly distributed between $0.9I_c$ and $1.1I_c$. The resulting phase diagram, for a single realization of disorder, is shown in Fig. 5. It is calculated using the same techniques as for ordered arrays. Once again, we see clear evidence of three phases: pinned lattice, plastic phase, and moving lattice. These have characteristics similar to those in the ordered case. For example, the moving lattice phase has a finite transverse critical current $i_{c\perp}$, which goes to zero near the phase boundary. In this 10×10 sample, there is an even larger finger of B phase interposed between A and C than there is in the ordered array; once again, we assume that this finger disappears in larger arrays. For strongly disordered square arrays at several different field strengths, a phase diagram resembling ours, though without the interpolated finger, has been found by Dominguez [13]. We have also calculated the voltage power spectra for the phases B and C ; they resemble those of Fig. 4 in that $P(\omega\tau)$ has peaks at multiples of a fundamental frequency in the moving lattice, while the spectra in the plastic phase are continuous and only weakly dependent on frequency.

IV. SIMPLIFIED ANALYTICAL MODELS

In a further effort to understand the behavior found numerically, we have considered two simple analytical models. In this section, we give a brief description of the models used. As will be seen, while each can reproduce *some* of the numerical results, neither generates all the details of the simulations.

A. Four-Plaquette Unit Cell

Our first analytical model is a slight generalization of an approach previously used by Rzchowski *et al* [19]. They consider the dynamics of a fully frustrated $N \times N$ array of overdamped resistively-shunted junctions. To treat this system analytically, they assume that the dynamical state is simply a periodic repetition of a square four-plaquette unit cell. It has long been known [20] that the ground state of the fully frustrated lattice has such a unit cell, corresponding to the checkerboard vortex pattern shown in Fig. 1. If we maintain this assumption of periodicity, the equations of Ref. [19] are readily extended to the case of currents applied at an angle to the plaquette edges. The resulting equations take the form

$$\gamma + \alpha + \beta + \delta = \pi(\text{mod}2\pi) \quad (10)$$

$$-\sin\beta - \frac{d\beta}{dt'} - \sin\delta - \frac{d\delta}{dt'} + \sin\gamma + \frac{d\gamma}{dt'} + \sin\alpha + \frac{d\alpha}{dt'} = 0 \quad (11)$$

$$\frac{d\gamma}{dt'} + \sin\gamma - \frac{d\alpha}{dt'} - \sin\alpha = I_{tot,x} \quad (12)$$

$$\frac{d\beta}{dt'} + \sin\beta - \frac{d\delta}{dt'} - \sin\delta = I_{tot,y} \quad (13)$$

where α , β , δ , and γ are the four inequivalent gauge-invariant phase differences describing the bonds of the 2×2 primitive cell (cf. Fig. 1 of Ref. [19]), $t' = t/\tau$ is a dimensionless time, and $I_{tot,x}$ and $I_{tot,y}$ are the total bias currents in the x and y directions per 2×2 superlattice cell (in units of the single-junction critical current).

We have solved these equations numerically, first reducing the system to three variables and then employing the same integration algorithm described above. In comparing with the equations for our first set of simulations, note that the quantity $I_{tot,\alpha} = 2i_\alpha$ ($\alpha = x, y$) is *twice* the current injected into each boundary grain. The resulting phase diagram is shown in Fig. 6. As in the previous phase diagrams calculated in this paper, there are regions (denoted A , B , and C) in which none, one, or both of the time-averaged voltages v_x and v_y are nonzero. Despite the reduction in number of variables and the enforced symmetry of this simulation, the voltages in regime C are still aperiodic in time, with continuous power spectra at most points in regime C . A representative power spectrum for $v_x(t')$ is shown in the inset to Fig. 6. It is calculated for a point in region C indicated by a triangle.

When the current is applied along the x axis, the critical current is close to the analytically computed [20] value $i_x = \sqrt{2} - 1$. By contrast, when $i_x \gg 1$, the boundaries of region B asymptotically approach the line $i_y = 1$. In general, we conclude that this simplified version of the dynamics has some, but not all, features of the large array. In particular it does have a region of “plastic flow” at large i_x and i_y . However, it fails to reproduce the region of plastic flow interposed between phases A and B and seen in our larger-scale simulations.

B. Single Vortex in an “Egg-Carton” Potential

Our second analytical model is even simpler. It refers, not to an entire lattice of vortices, but to a *single* vortex moving in the “egg-carton” potential formed by the lattice. According to Lobb, Abraham, and Tinkham [18], a single vortex can be viewed, to a good approximation, as moving in a potential of the form

$$V(x, y) = -V_0 \left[\cos\left(\frac{2\pi x}{a}\right) + \cos\left(\frac{2\pi y}{a}\right) \right], \quad (14)$$

where a is the lattice constant of the array and V_0 is the depth of the potential felt by a single vortex. This potential has minima at $\mathbf{r} \equiv (x, y) = (n_1 a, n_2 a)$ where $n = 0, \pm 1, \pm 2, \dots$. [The grains of the Josephson lattice, in these coordinates, are located at $((n_1 + \frac{1}{2})a, (n_2 + \frac{1}{2})a)$, and correspond to *maxima* of the vortex potential.]

The current-voltage characteristics of this model are readily calculated. The Magnus force on a vortex due to an external current density \mathbf{J} may be written (taking \hat{z} as the direction perpendicular to the array)

$$\mathbf{F}_{ext} = \Phi_0 \hat{z} \times \mathbf{J}/c, \quad (15)$$

where \mathbf{J} , in this two-dimensional system, represents a current per unit *length*. In the steady state, this force has to be balanced by two other forces: the gradient of the egg-carton potential energy and the frictional force experienced by the vortex moving through the lattice. This condition may be written

$$\mathbf{F}_{ext} - \nabla V(\mathbf{r}) - \eta \dot{\mathbf{r}} = 0, \quad (16)$$

or explicitly, in component form,

$$\eta\dot{x} = -\frac{\Phi_0 J_y}{c} - \frac{2\pi}{a} V_0 \sin\left(\frac{2\pi x}{a}\right) \quad (17)$$

$$\eta\dot{y} = \frac{\Phi_0 J_x}{c} - \frac{2\pi}{a} V_0 \sin\left(\frac{2\pi y}{a}\right). \quad (18)$$

Given the vortex velocities, the electric fields may be written down by using the relation between vortex velocity and electric field. Specifically, the voltage drop between any two points P_1 and P_2 is given by

$$\Delta V_{12} = 2\pi n v_{\perp} L \frac{\hbar}{2e}, \quad (19)$$

where v_{\perp} is the component of vortex velocity perpendicular to the line joining P_1 and P_2 , L is the distance between P_1 and P_2 , and n is the vortex number density per unit area. Here we have used the fact that the phase difference between P_1 and P_2 changes by 2π every time a vortex crosses that line, and have also availed ourselves of the Josephson relation between voltage and phase. We therefore deduce the following expressions for the components of electric field:

$$E_x = \frac{\hbar n \dot{y}}{2e} \quad (20)$$

$$E_y = -\frac{\hbar n \dot{x}}{2e}. \quad (21)$$

Eqs. (17) and (18) are identical in form to the equations for single Josephson junctions, with x/a and y/a playing the role of the Josephson phase, $2\pi V_0/a$ the role of the critical current, and $-\Phi_0 J_y/c$ and $\Phi_0 J_x/c$ the roles of the driving currents. In view of eqs. (17) and (18), we deduce that the time-averaged voltage drop in the i direction ($i = x, y$) becomes nonzero when $|\Phi_0 J_i/c| > 2\pi V_0/a$. As has been shown by ref. [18], V_0 is related to the critical current I_c of an individual Josephson junction by

$$V_0 \sim 0.22 \frac{\hbar I_c}{2e}. \quad (22)$$

Collecting all this information, we obtain the simple phase diagram shown in Fig. 7 for the voltage drops arising from motion of a single vortex in a square array. Once again, there are three regimes, denoted A , B , and C , where none, one, or both of the time-averaged voltage drops $\langle v_x \rangle_t$ and $\langle v_y \rangle_t$ are nonzero. However, the phase diagram is simplified by the fact the $\langle v_x \rangle_t$ and $\langle v_y \rangle_t$ are independent of one another, depending only on i_x and i_y respectively. The phase boundaries correspond to the vertical and horizontal lines $v_x \sim 0.11$ and $v_y \sim 0.11$.

The results of Fig. 7 are obviously oversimplified compared to the numerical diagrams of Fig. 2. In addition to the other obvious differences, the voltages in region C are not chaotic, but are instead just the superposition of two independent voltages in the x and y directions, each of which has its own fundamental frequency and harmonics of that fundamental. The two fundamentals may, of course, be incommensurate depending on the values of $\langle v_x \rangle_t$ and $\langle v_y \rangle_t$.

V. DISCUSSION AND CONCLUSIONS

The present calculations clearly show that a fully frustrated array of overdamped Josephson junctions exhibits at least three dynamical phases as a function of the two orthogonal driving currents i_x and i_y : a pinned vortex lattice, a plastic phase characterized by a continuous power spectrum for both v_x and v_y , and a moving vortex lattice with only one of the voltages v_x and v_y nonzero. In this last phase, the power spectrum, at least for the limited lattice sizes we have investigated, contains only harmonic multiples of a fundamental frequency. Weak disorder in the critical currents appears not to change this phase diagram greatly.

Regarding our phase diagram, it is natural to ask whether the boundaries between the different phases are analogous to first-order phase transitions. Although we have no conclusive evidence, our numerical results suggest that they may indeed be first-order, rather than continuous, at least for the ordered lattices. In support of this conjecture, we note the occasional occurrence of hysteresis in our simulations, and of discontinuous jumps between one phase and another near the phase boundaries. There is also little evidence that any quantities, such as the strength of the voltage noise, diverge near the phase boundaries, as might be expected of a continuous phase transition. In this respect, these transitions differ somewhat from those seen in strongly disordered lattices.

For these ordered arrays in which the vortex lattice is commensurate with the underlying Josephson array, one might have expected other types of commensurate-incommensurate transitions as the angle between the applied current and array symmetry axis is varied. Such “magic angle” effects, with a multitude of commensurate and disordered phases, are seen in other models in which vortex lattices are driven through periodic pinning arrays [9,10]. In the present case, we have seen no clear evidence of any phases other than the three shown in our phase diagram. Possibly, such additional phases would appear if we studied larger arrays in which such delicate effects would be more stable. On the other hand, our open boundary conditions may constitute such a strong perturbation on the periodic array that such commensurability effects would be suppressed even for very large lattices.

Finally, we comment briefly on the power spectra found in our simulations. In the moving lattice phase B , the voltage power spectra appear to contain only multiples of a fundamental frequency. Such a power spectrum represents an array which is phase-locked, and hence would radiate power only at multiples of that fundamental frequency. In this case, phase-locking clearly occurs *between* rows as well as *along* rows of junctions parallel to the voltage. Such phase locking must be present because it is required in order to produce the observed relation between $\langle v_x \rangle_t$ and the fundamental frequency. Furthermore, such locking survives weak disorder in the critical currents. The effectiveness of a magnetic field in producing phase locking in square arrays has been discussed previously [21,22]. The present work provides additional evidence that a field $f = 1/2$ is effective in producing phase locking, even when the applied current has nonzero components parallel to both array axes [23].

In conclusion, we have numerically investigated the dynamic phases of fully-frustrated square Josephson junction arrays driven by two independent, orthogonal currents. We find three phases: stationary lattice, driven lattice, and plastic flow. These phases appear also in weakly disordered arrays. We find that our numerical results can be partly understood by two simple analytical models, which show some of the features of the full simulation.

VI. ACKNOWLEDGMENTS

This work has been supported by the National Science Foundation, Grant No. DMR97-31511, and by the Midwest Superconductivity Consortium at Purdue University through Grant DE-FG 02-90 ER45427. We thank Profs. Predrag Cvitanovic and Franco Nori for useful conversations.

-
- [1] S. Bhattacharya and M. J. Higgins, Phys. Rev. B **52**, 64 (1995).
 - [2] U. Yaron, P. L. Gammel, D. A. Huse, R. N. Kleinman, C. S. Oglesby, E. Bucher, B. Batlogg, D. J. Bishop, K. Mortensen, K. Clausen, C. A. Bolle, and F. De La Cruz, Phys. Rev. Lett. **73**, 2748 (1994).
 - [3] M. Marchevsky, J. Aarts, P. H. Kes, and M. V. Indenbom, Phys. Rev. Lett. **78**, 531 (1997).
 - [4] M. C. Hellerqvist, D. Ephron, W. R. White, M. R. Beasley, and A. Kapitulnik, Phys. Rev. Lett. **76**, 4022 (1996).
 - [5] W. Henderson, E. Y. Andrei, M. J. Higgins, and S. Bhattacharya, Phys. Rev. Lett. **77**, 2077 (1996).
 - [6] N. R. Dilley, J. Herrmann, S. H. Han, and M. B. Maple, Phys. Rev. B **56**, 2379 (1997).
 - [7] L. Balents, M. C. Marchetti, L. Radzihovsky, Phys. Rev. B **57**, 7705 (1998).
 - [8] S. Spencer and H. J. Jensen, Phys. Rev. B **55**, 8473 (1997).
 - [9] C. Reichhardt, C. J. Olson, and Franco Nori, Phys. Rev. **B58**, 6534 (1998); C. Reichhardt, C. J. Olson, and Franco Nori, Phys. Rev. **B57**, 7937 (1998); C. Reichhardt, C. J. Olson, and F. Nori, Phys. Rev. Lett. **78**, 2648 (1997).
 - [10] C. Reichhardt and Franco Nori, Phys. Rev. Lett. **82**, 414 (1999).
 - [11] S. Ryu, M. Hellerqvist, S. Doniach, A. Kapitulnik, and D. Stroud, Phys. Rev. Lett. **77**, 5114 (1996).
 - [12] For reviews of this work, see, e. g., the articles and references in *The Kosterlitz-Thouless Transition and Superconducting Arrays*, edited by D. Kim, J. S. Chung, and M. Y. Choi (Min Eum Sa, Seoul, 1993).
 - [13] D. Dominguez, Phys. Rev. Lett. **82**, 181 (1999). See also D. Dominguez, N. Gronbech-Jensen, and A. R. Bishop, Phys. Rev. Lett. **78**, 2644 (1997).
 - [14] L. Balents and M. P. A. Fisher, Phys. Rev. Lett. **75**, 4270 (1995).
 - [15] Wenbin Yu, K. H. Lee, D. Stroud, Phys. Rev. B **47** 5906 (1993).
 - [16] J. R. Cash and Alan Karp, ACM Trans. Math. Software **16** 201 (1990).
 - [17] W. H. Press, S. A. Teukolsky, W. T. Vetterling, and B. P. Flannery, *Numerical Recipes in C (2nd ed.)* (Cambridge, 1992), Chap. 13, Sec. 8.
 - [18] C. J. Lobb, D. W. Abraham, and M. Tinkham, Phys. Rev. **B27**, 150 (1983).
 - [19] M. S. Rzchowski, L. L. Sohn, and M. Tinkham, Phys. Rev. **B43**, 8682 (1991).
 - [20] S. Teitel and C. Jayaprakash, Phys. Rev. **B27**, 598 (1983).

- [21] G. Filatrella and K. Wiesenfeld, J. Appl. Phys. **78**, 1878 (1995).
- [22] B. R. Trees and D. Stroud, Phys. Rev. **B59**, 7108 (1999).
- [23] Aranson *et al* [I. Aranson, S. Scheidl, and V. M. Vinokur, Phys. Rev. **B58**, 14541 (1998)] have recently shown that the moving vortex lattice phase, in the presence of weak disorder, must eventually become unstable with respect to a proliferation of dislocations at large enough lattice sizes or high enough velocities.

FIG. 1. Schematic of the geometry for calculating IV characteristics. Currents $i_x = I_x/I_c$ and $i_y = I_y/I_c$ are injected into each grain (shaded circles) on left-hand and lower edges of the square array, and extracted from right-hand and upper edges, as shown. Time-dependent but spatially averaged voltage drops $v_x(t')$ and $v_y(t')$ are calculated across the array in the x and y directions. Crosses denote vortex locations, as defined in the text, for the ground-state checkerboard pattern at $f = 1/2$.

FIG. 2. Calculated zero-temperature “dynamical phase diagram” for (a) 10×10 and (b) 20×20 square Josephson arrays with currents applied in both the x and y directions. Region *A*: pinned vortex lattice ($\langle v_x \rangle_t = \langle v_y \rangle_t = 0$). Region *B*: moving vortex lattice phase ($\langle v_x \rangle_t = 0, \langle v_y \rangle_t > 0$, or $\langle v_y \rangle_t = 0, \langle v_x \rangle_t > 0$). Region *C*: moving plastic vortex phase ($\langle v_x \rangle_t > 0, \langle v_y \rangle_t > 0$). The phase boundaries were determined numerically at the calculated points, as described in the text; the smooth lines are interpolations between these points. The phase diagram is assumed symmetric about a 45° line; diamonds denote points which were calculated for $i_x > i_y$; circles, for $i_y > i_x$. The sliver of phase *C* between *A* and *B* in (a) is a finite-size artifact, as shown in (b) where it is seen to be absent in a 20×20 array. Open triangles in (b) indicate currents (i_x, i_y) at which the voltage traces and power spectra of Figs. 3 and 4 were calculated.

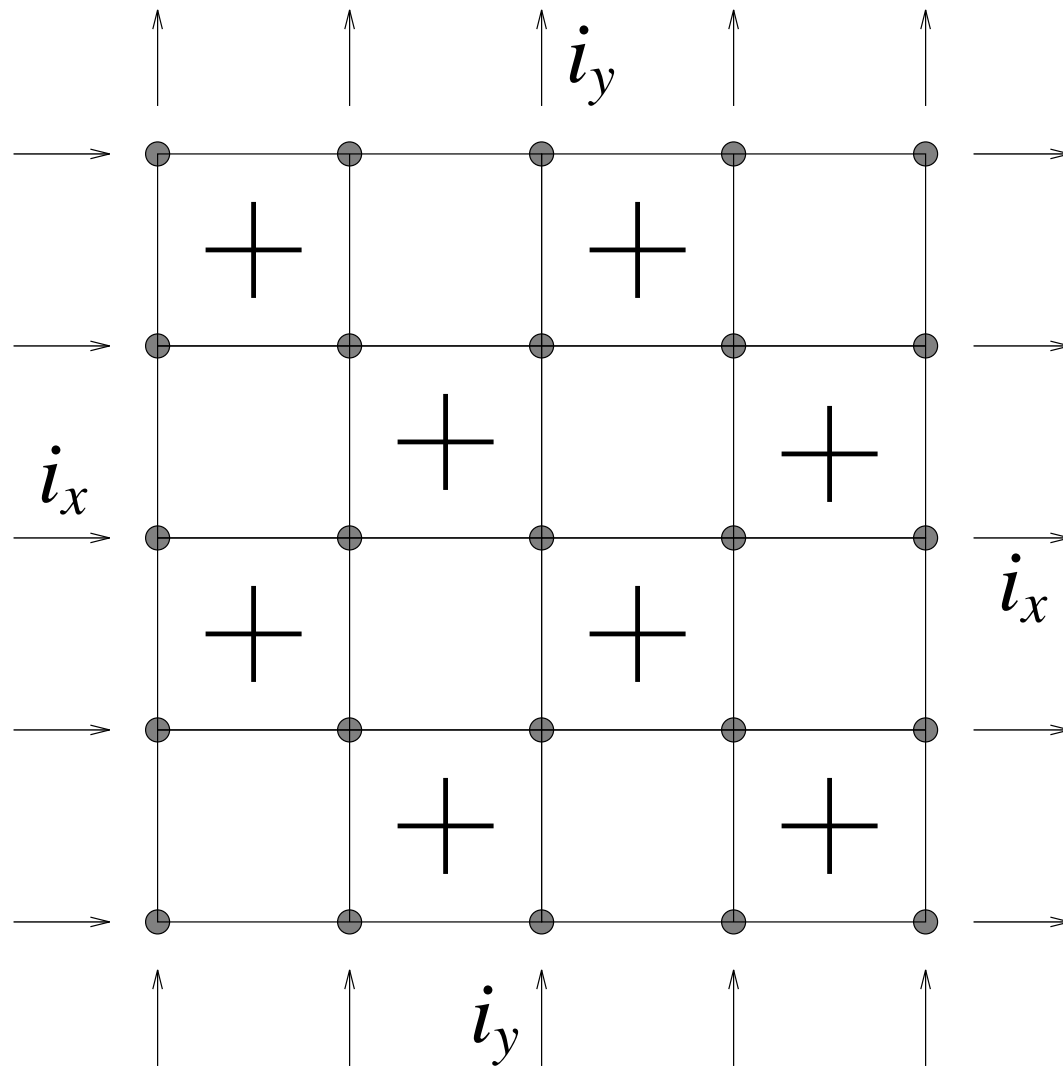
FIG. 3. Time-dependent voltage traces $v_x(t')$ and $v_y(t')$ (upper and lower parts of each panel) for several points in the phase diagram of a 20×20 array at $f = 1/2$. (a) $[i_x = 0.351, i_y = 0.079]$ and (b) $[i_x = 405, i_y = 0.294]$, represent points in the plastic phase *C*; (c) $[i_x = 0.508, i_y = 0.210]$ and (d) $[i_x = 0.469, i_y = 0.287]$ are points in the moving-lattice phase *B*. As described in the text, $v_x(t')$ represents the difference between the average voltages on the left-hand and right-hand edge of the array; $v_y(t')$ is the difference between the average voltages on the top and bottom edges of the array. $t' = t/\tau$ is a dimensionless time; τ is a natural time unit defined in the text.

FIG. 4. Calculated voltage power spectra $P(\omega\tau)$ for the voltages $v_x(t')$ and $v_y(t')$ of Fig. 3 (a) - (d). Here ω is the angular frequency. In each panel, the power spectrum for v_x lies above that for v_y .

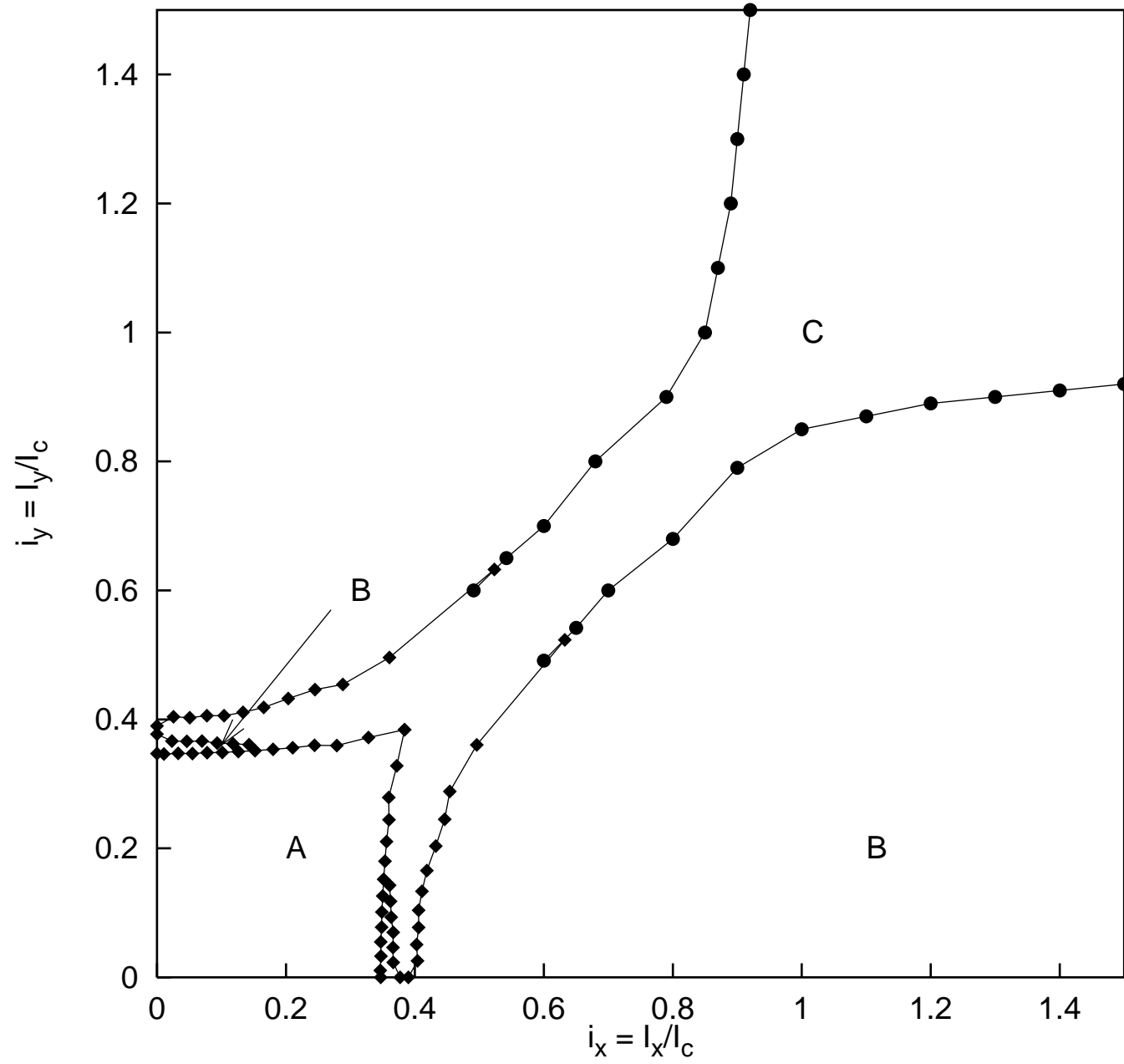
FIG. 5. Calculated phase diagram for a 10×10 array at $f = 1/2$ with one realization of weak disorder. Rather than all being equal, the critical currents are chosen at random from a distribution which is uniform in the interval $(0.9I_c, 1.1I_c)$.

FIG. 6. Calculated phase diagram for a square array at $f = 1/2$, obtained by solving the overdamped dynamical equations for a 2×2 unit cell which is assumed to be repeated throughout the lattice [eqs. 10-13]. The phase diagram is shown as a function of the driving currents i_x and i_y in the x and y directions. As in previous phase diagrams, there are regions where none, one, or both of the two time-averaged voltages $\langle v_x \rangle_t$ and $\langle v_y \rangle_t$ are nonzero. Inset shows power spectrum of $v_x(t')$ for the point indicated by the open triangle ($i_x = 1.348, i_y = 1.115$).

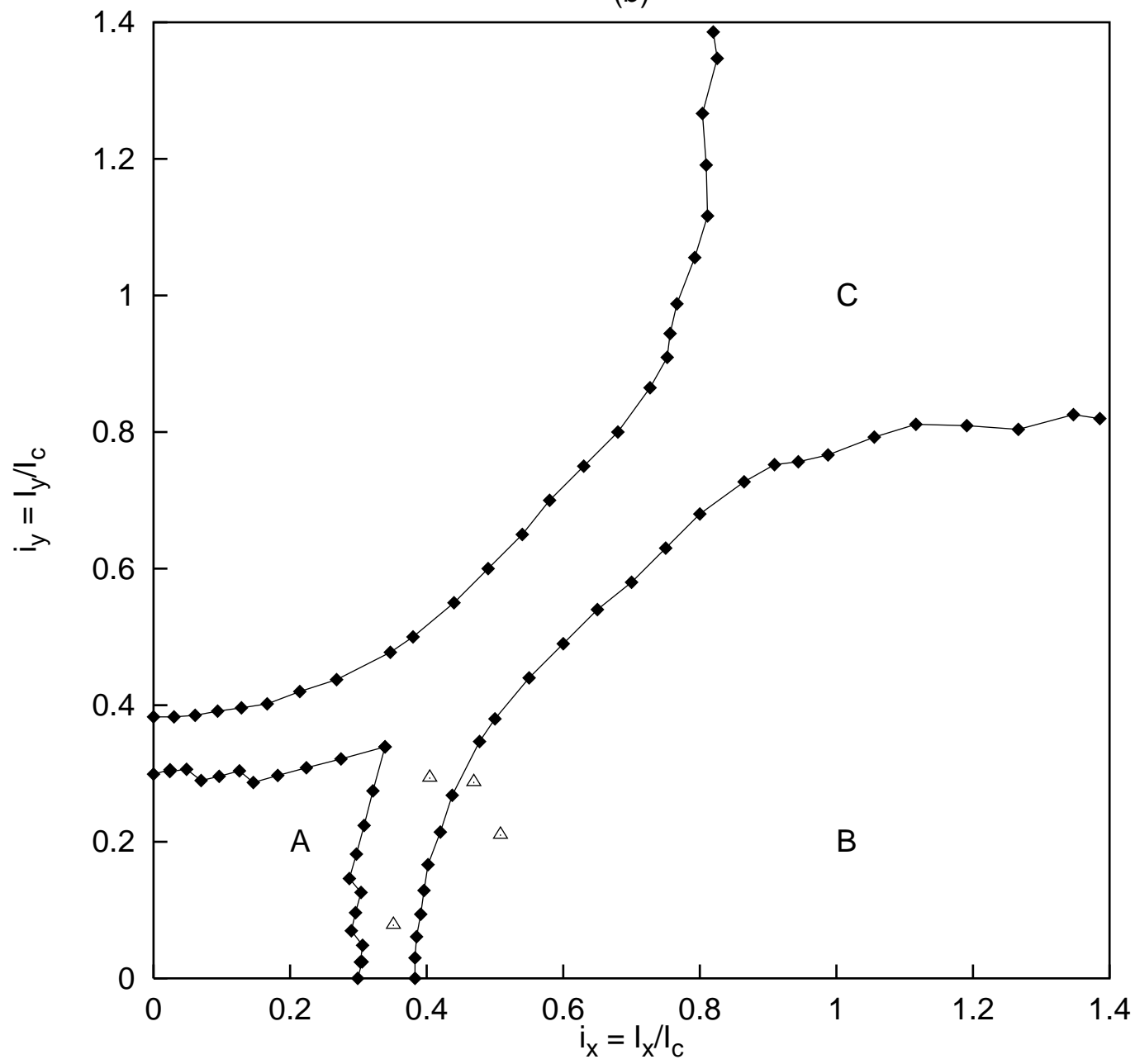
FIG. 7. Calculated phase diagram for a single vortex moving in the egg-carton potential produced by a square array of overdamped Josephson junctions. The notation is the same as in Fig. 6. Once again, there are regions where none, one, or both of the time averaged voltages $\langle v_x \rangle_t$ and $\langle v_y \rangle_t$ are nonzero.

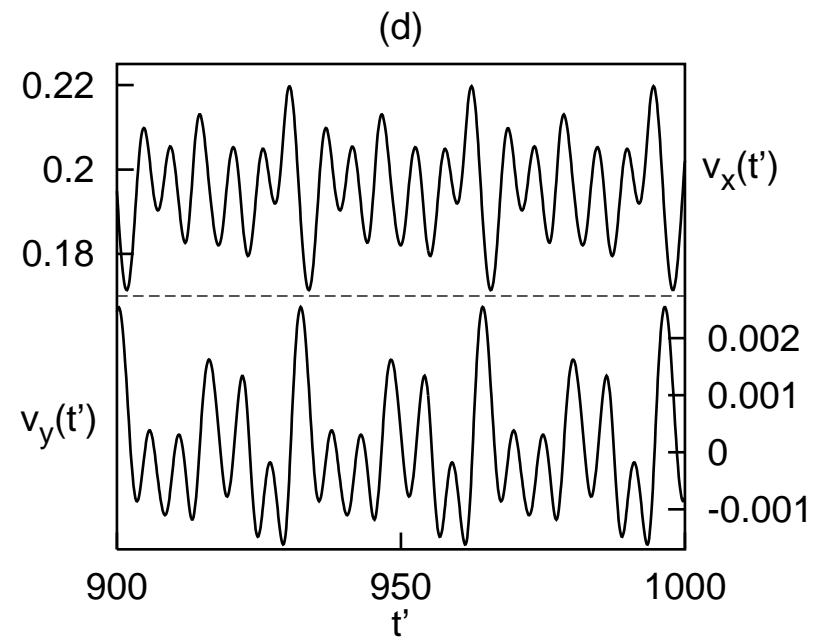
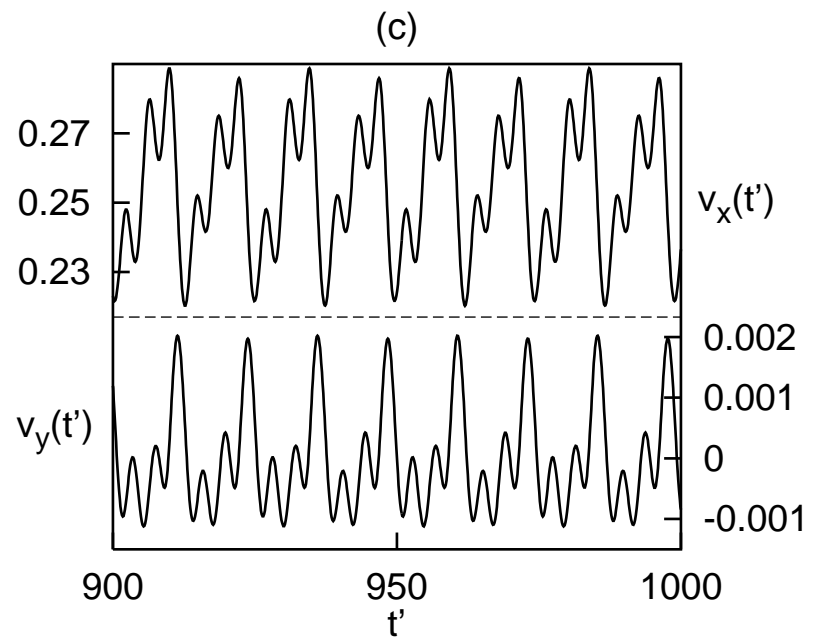
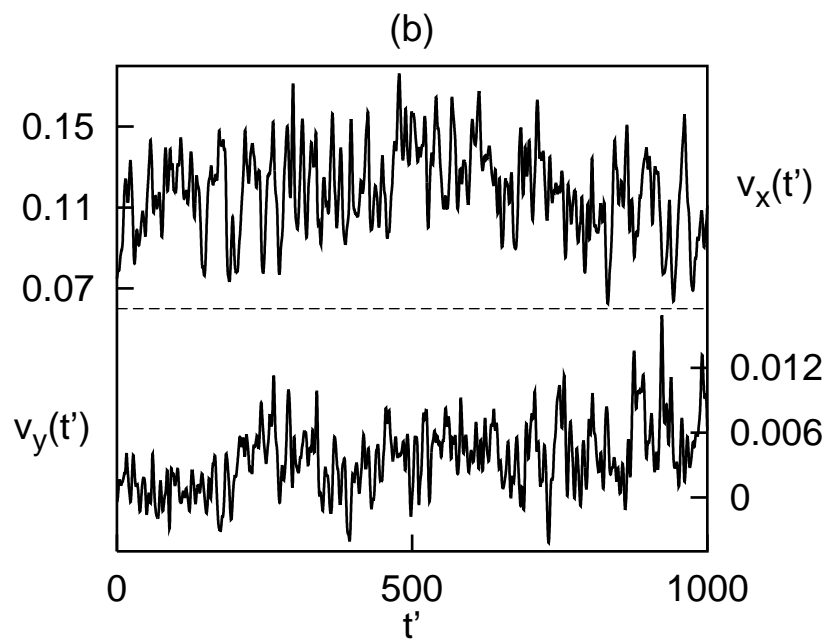
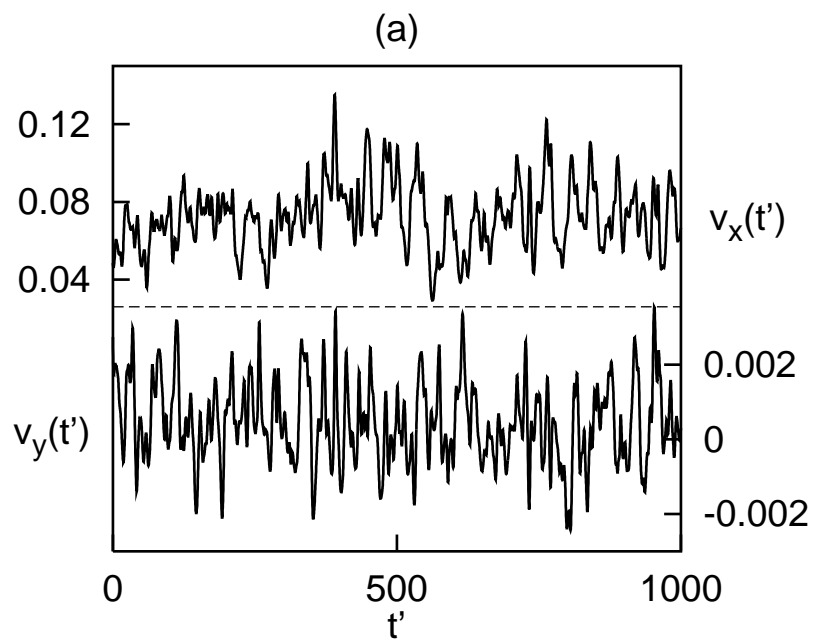


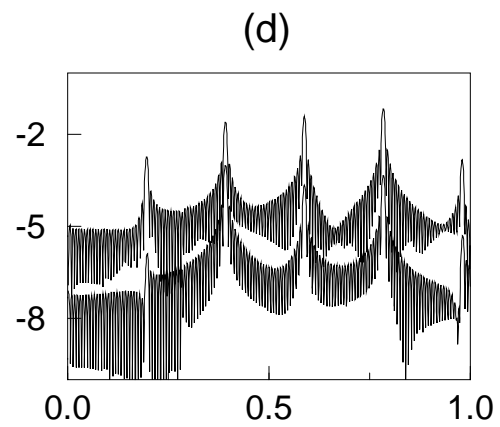
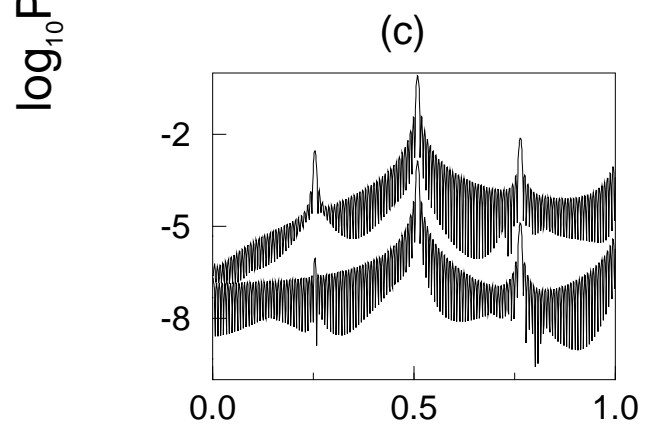
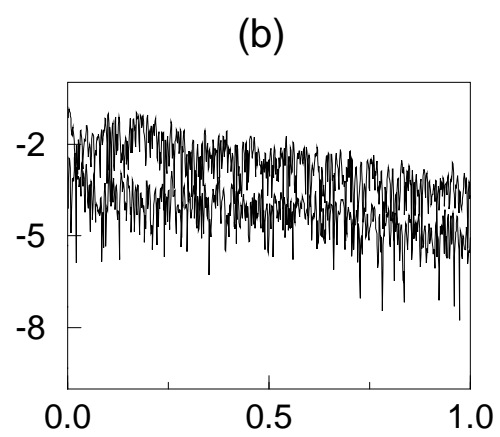
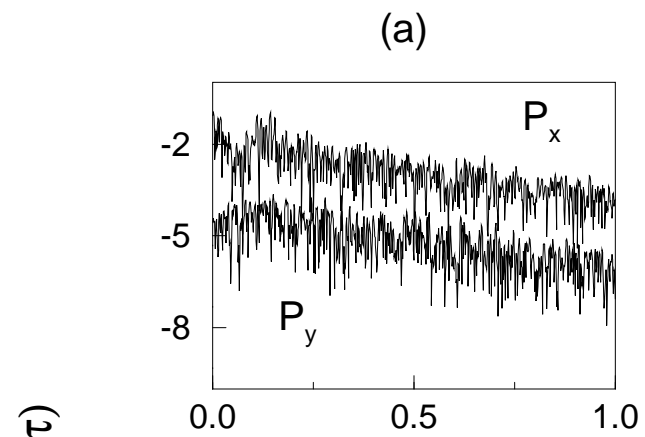
(a)



(b)







$\omega\tau$

